

## The isotopic and hydrologic response of small, closed-basin lakes to climate forcing from predictive models: Application to paleoclimate studies in the upper Columbia River basin

Byron A. Steinman,\* Michael F. Rosenmeier, Mark B. Abbott, and Daniel J. Bain

Department of Geology and Planetary Science, University of Pittsburgh, Pittsburgh, Pennsylvania

### *Abstract*

Simulations conducted using a coupled lake-catchment, hydrologic and isotope mass-balance model indicate that small, closed-basin lakes in north-central Washington are isotopically sensitive to changes in precipitation, relative humidity, and temperature. Most notably, model simulations predicted inconsistent lake responses to precipitation changes due to differences in lake outseepage rates and surface area to volume (SA:V) ratios. Greater outseepage within model experiments resulted in increased sensitivity to changes in mean precipitation. Moreover, simulations suggest that, in lakes with appreciable outseepage, SA:V ratio changes resulting from lake-level variations control the direction of changes in lake water oxygen isotope composition ( $\delta^{18}\text{O}$ ). Specifically, in lakes with a SA:V ratio that increases at higher lake levels, steady state  $\delta^{18}\text{O}$  values will increase in response to greater long-term average precipitation. These results suggest that closed-basin lakes with low outseepage rates will exhibit a transient isotopic response to stochastic variability in hydrologic forcing but will not strongly respond at steady state to variation in mean hydrologic conditions. Conversely, closed-basin lakes with appreciable outseepage will exhibit strong isotopic responses to both stochastic variability and variation in mean hydrologic conditions (i.e., mean precipitation, relative humidity, and temperature control of catchment hydrologic inputs to the lake). These relationships provide a mechanism for explaining inconsistencies in the isotopic responses of lakes within a given region to hydrologic forcing and demonstrate that semiquantitative models for describing the relationship between lake hydrologic and isotopic responses to climate variability are not appropriate for all closed-basin lakes.

The hydrologic and chemical evolution of a lake is subject to a complex array of climate and catchment controls that can be mathematically described and related using numeric mass-balance models. Previous modeling studies have examined the influence of changes in climate (relative humidity, precipitation, temperature, solar insolation, wind speed, etc.) on the isotopic composition of lake water by simulating hydrologic and isotopic fluxes through time (Hostetler and Benson 1994; Gibson et al. 2002; Shapley et al. 2008). These climate variables, as well as catchment parameters and basin morphology, control water balance and lake residence time, and therefore define the temporal extent and magnitude of lake responses to climate dynamics. As such, mass-balance models can be used both to interpret lake sediment oxygen isotope ( $\delta^{18}\text{O}$ ) records by characterizing lake sensitivity to specific climate variables and to investigate underdetermined aspects of lake hydrologic systems (such as outseepage and through-flow rates) and therefore are useful to both paleoclimatologists (Rowe and Dunbar 2004; Jones et al. 2007; Rosenmeier et al. in press) and water resources scientists (Sacks 2002).

In the seasonal, drought-prone climate of north-central Washington, small, closed-basin lakes (i.e., lakes with low rates of outseepage and no surficial outflow) exhibit hydrologic and isotopic instability. This instability arises primarily from the inflow of isotopically light surface runoff from snowmelt and spring precipitation and from

evaporative enrichment of isotopes throughout the summer and early fall. In these lakes, the low salinity and isotopic depletion of runoff results in early spring water column stratification that is then weakened by wind action, diffusion, and evaporative enrichment in subsequent months. The persistent isotopic and chemical instability of closed-basin lakes in north-central Washington precludes the application of standard steady state analytical models and necessitates the use of numerical models to quantitatively describe lake response to climate change.

In this paper, a coupled lake and catchment numeric mass-balance model is presented that simulates the hydrologic and isotopic response of two small, closed-basin lakes, Castor Lake and Scanlon Lake, to changes in the primary drought controlling climate variables (i.e., precipitation, relative humidity, and temperature). This relatively simple model is similar to the (hydrologic–isotopic balance (HIBAL) model for application to paleolake systems) model of Benson and Paillet (2002) in that it incorporates observed mixing depths and meteorological data to predict near surface and deeper lake water isotopic and hydrologic responses to climate forcing. To account for hydrologic inputs directly from the surrounding catchment (a component not represented in the HIBAL system) the model presented here incorporates catchment subroutines that describe snowpack, runoff, and soil moisture volume changes through time. Of the more sophisticated coupled lake-catchment models that are well established in the literature (e.g., the calibration free, one-dimensional thermal model of Hostetler and Bartlein 1990),

\* Corresponding author: bas68@pitt.edu

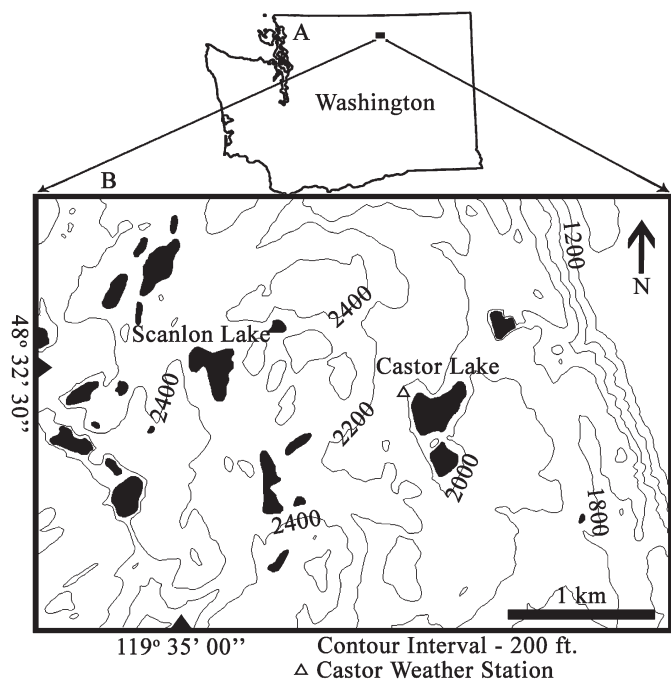


Fig. 1. (A) Map of Washington State showing the approximate location of the study area. (B) Topography of the Castor and Scanlon Lake catchments and surrounding area.

none are applicable to nonfreshwater lakes because they do not account for changes in solute concentrations, an important driver of seasonal lake stratification in oligosaline and mesosaline lakes such as Castor and Scanlon. The model presented here is structured to be computationally simple and applicable to a much wider range of lake types, particularly small, closed systems in seasonal climates with stratification regimes influenced by salinity changes.

The Castor and Scanlon Lake model simulations presented here used meteorological data from local and regional weather stations, catchment area and soil survey data, and lake depth and  $\delta^{18}\text{O}$  values as initial conditions (i.e., initial model variable inputs). Catchment models for each lake were calibrated by adjusting an inflow delay constant until differences between model estimates obtained using continuous weather station data and measured monthly lake levels and surface water  $\delta^{18}\text{O}$  values from the same period (June 2005 to December 2008) were minimized. Following calibration, model simulations were conducted to determine lake sensitivity to changes in temperature, relative humidity, and precipitation and to describe the potential for variations in outseepage and hypsography to affect lake water isotopic composition.

## Methods

**Study sites**—Scanlon Lake (SL) and Castor Lake (CL) are located in the “lime belt region” of Okanogan County, Washington, on a terrace margin of the Okanogan River (Fig. 1). The landscape is characterized by shrub-steppe, evergreen, and secondary deciduous vegetation, and numerous small, perched lakes and seasonal wetlands.

Table 1. CL and SL hydrologic model parameters and initial values for the continuous input (2005–2008) simulations.

Catchment parameters	Value		Reservoir	Initial value ( $\text{m}^3$ )	
	CL	SL		CL	SL
$CA$ ( $\text{km}^2$ )	0.86	0.49	$RES_{SL}$	216,000	120,000
$AWC_{SS}$ (cm)	2.3	2.3	$RES_{DL}$	77,500	10,000
$AWC_{DS}$ (cm)	2.3	2.3	$RES_{SS}$	0	0
$C_{IN}$	0.21	0.21	$RES_{DS}$	0	0
$C_{SR}$	0.016	0.007	$RES_{IN}$	10,000	2500
			$RES_{SP}$	0	0

Bedrock is principally limestone with mixed calcareous sedimentary rock. Like most small lakes in this region, CL and SL are kettle lakes that formed during the retreat of the late Pleistocene Cordilleran ice sheet. The lake catchments are small ( $< 1 \text{ km}^2$ ; Table 1) and occupy a topographic high isolated from regional groundwater. Lake salinity varies with depth and season between  $\sim 1$  and  $4 \text{ mS cm}^{-2}$  and 3 and  $20 \text{ mS cm}^{-2}$  for CL and SL, respectively. No evidence exists for organized drainage at SL, and overflow occurs along the northeastern margin of CL only in the spring of very wet years. As a consequence, evaporative losses control the hydrologic balance of both lakes (Fig. 2).

The seasonal, semiarid climate of north-central Washington is largely controlled by interactions between the Pacific westerlies and the Aleutian low pressure and north Pacific high-pressure systems (Brynton and Hare 1974). In the winter months, the Aleutian low strengthens and moves southward, bringing cool, moist air to the Washington coast. In the summer months, the Aleutian low weakens, moves northward, and is replaced by the north Pacific high. These winter (cool, moist) and summer (warm, dry) air masses are pushed eastward, over the Cascade Mountains,

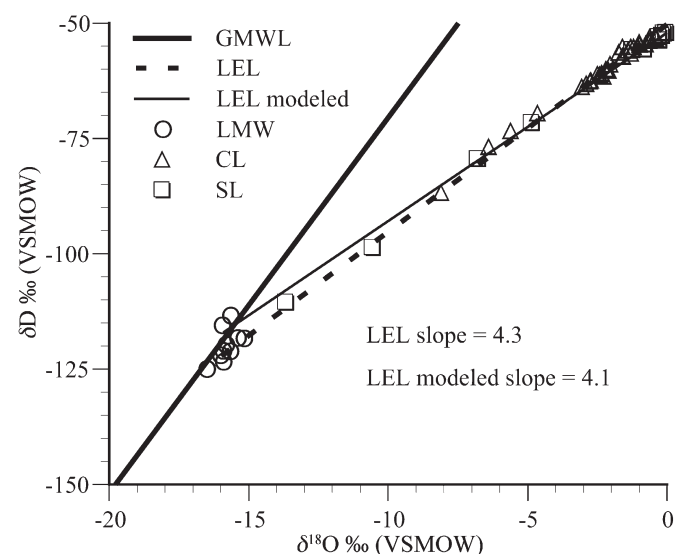


Fig. 2. Global meteoric water line (GMWL), measured  $\delta^{18}\text{O}$  and  $\delta D$  values for Castor Lake (open triangles) and Scanlon Lake (open squares) surface waters, local meteoric waters (LMW, open circles), and slopes of observed and modeled local evaporation lines (LEL and LEL modeled, respectively).

by the Pacific westerlies, leading to a highly seasonal and interannually variable climate (Table 2).

*Model structure*—The hydrologic and isotope mass balance of a lake can be described by the following equations:

$$\frac{dV_L}{dt} = \Sigma I - \Sigma O \tag{1}$$

$$\frac{d(V_L \delta_L)}{dt} = \Sigma I \delta_I - \Sigma O \delta_O \tag{2}$$

where  $V_L$  is lake volume,  $\Sigma I$  and  $\Sigma O$  are the total surface and below ground inflows to and outflows from a lake, and  $\delta$  is the isotopic composition of the inflows and outflows. These equations provide the basis for a hydrologic and isotope mass-balance model that is defined by a system of 12 ordinary differential equations compiled using Stella (Isee Systems) software. Specifically, the model equations, as well as variables and parameters (Table 3), integrate a system of lake and catchment water reservoirs (notated as *RES* in the equations that follow) and volumetric fluxes ( $F$ ) to the reservoirs, including a two-layer (surface and deep) model subroutine for soil moisture availability and a two-layer (surface and deep) subroutine for lake stratification described by separate differential equations. Snowpack and inflow reservoirs are also used to simulate water transfer delays associated with winter freezing and water mass travel time along slower flow paths.

*Hydrologic mass-balance equations*—The model calculates mass balance through time for near surface and deep lake waters ( $RES_{SL}$  and  $RES_{DL}$ , respectively) by the volumetric addition of direct precipitation over the lake area ( $F_P$ ) and inflow from the catchment ( $F_{IN}$ ), and subtraction of lake water evaporation ( $F_E$ ) and outseepage through shallow lake and deep lake sediments ( $F_{SOS}$  and  $F_{DOS}$ ). Lake water mass balance is also controlled by surface and deep water mixing fluxes ( $F_{SLM}$  and  $F_{DLM}$ , respectively) associated with the establishment and breakdown of lake stratification (Eqs. 18, 19). Within Stella, the lake water mass balance is described by the following equations, using the notation above:

$$\frac{dRES_{SL}}{dt} = F_P + F_{IN} + F_{DLM} - F_E - F_{SLM} - F_{SOS} \tag{3}$$

$$\frac{dRES_{DL}}{dt} = F_{SLM} - F_{DLM} - F_{DOS} \tag{4}$$

where direct precipitation over the lake surface area (again,  $F_P$ ,  $F_P = F_{SF} + F_R$ ) is specifically determined by monthly and/or daily precipitation inputs (*see* Model inputs, below). Evaporation from the lake surface, in turn, is estimated by a combination radiation-aerodynamic Penman equation (Eq. 22).

Soil water mass balance is determined by the amount of rainfall and snowmelt over the catchment surface area (excluding the lake surface area;  $F_R$  and  $F_{SM}$ , Eqs. 9, 10), catchment evapotranspiration (Eqs. 12, 23), infiltration

Table 2. Monthly model input data.

Month	Precipitation* (mm)	Temperature* (°C)	RH† (%)	Solar rad. (MJ m <sup>-2</sup> d <sup>-1</sup> )	Wind speed‡ (m s <sup>-1</sup> )	δ <sup>18</sup> O <sub>P</sub> (‰)	δD <sub>P</sub> (‰)	Stratification depth (m)		Lake-air temperature offset (°C)	
								CL	SL	CL	SL
Jan	34	-4.3	84	2.5	1.3	-15.7	-119	0	0	9.2	7.3
Feb	29	-1.4	77	6.1	1.3	-15.1	-118	0	0	4.1	2.2
Mar	24	3.7	64	12.2	1.5	-15.2	-113	0	0	2.8	2.2
Apr	23	8.5	56	22.3	1.5	-12.9	-96	0.5	0.5	5.2	9.8
May	27	12.6	56	26.4	1.5	-10.6	-82	1.5	1.5	2.5	8.7
Jun	31	16.2	54	30.9	1.4	-10.2	-84	3.25	3.25	4.3	7.8
Jul	14	19.6	46	31.3	1.4	-10.0	-81	6.0	5.0	2.5	4.0
Aug	12	18.9	48	25.1	1.3	-10.6	-86	6.0	5.0	2.5	3.1
Sep	13	14.3	54	16.5	1.3	-9.8	-76	6.0	5.0	3.5	3.4
Oct	20	7.8	67	8.7	1.2	-12.0	-88	6.0	5.0	4.7	3.7
Nov	36	1.0	81	3.6	1.2	-14.4	-111	0	0	5.3	3.3
Dec	45	-3.0	86	2.2	1.2	-15.7	-116	0	0	6.2	3.8
Coefficient of variation;‡	0.28	0.12	0.06	0.04	0.06						

\* Average from Omak and Conconully NCDC weather stations (1900–2007).

† Average from Omak AgriMet weather station (1989–2007).

‡ Coefficient of variation of the annual average over the period of measurement.

Table 3. Model variables and parameters.

$RES_{SL}$	Surface lake reservoir, m <sup>3</sup>	$AWC_{SS}$	Available water capacity surface soil, m
$RES_{DL}$	Deep lake reservoir, m <sup>3</sup>	$AWC_{DS}$	Available water capacity deep soil, m
$RES_{SS}$	Surface soil reservoir, m <sup>3</sup>	$PET$	Potential evapotranspiration, m month <sup>-1</sup>
$RES_{DS}$	Deep soil reservoir, m <sup>3</sup>	$C_{IN}$	Catchment inflow delay constant, unitless
$RES_{IN}$	Inflow reservoir, m <sup>3</sup>	$SVC$	Surface lake volume control, m <sup>3</sup>
$RES_{SP}$	Snowpack reservoir, m <sup>3</sup>	$C_{SR}$	Seepage constant, unitless
$F_P$	Precipitation on the lake surface, m <sup>3</sup> month <sup>-1</sup>	$ALB$	Lake surface albedo, unitless
$F_{IN}$	Catchment inflow to the lake, m <sup>3</sup> month <sup>-1</sup>	$R_s$	Solar radiation, MJ m <sup>-2</sup> d <sup>-1</sup>
$F_E$	Evaporation from the lake surface, m <sup>3</sup> month <sup>-1</sup>	$R_a$	Extraterrestrial solar radiation, MJ m <sup>-2</sup> d <sup>-1</sup>
$F_{SOS}$	Shallow lake outseepage, m <sup>3</sup> month <sup>-1</sup>	$RH$	Relative humidity, %
$F_{DOS}$	Deep lake outseepage, m <sup>3</sup> month <sup>-1</sup>	$a_u$	Penman wind function constant, unitless
$F_{SLM}$	Shallow lake mixing, m <sup>3</sup> month <sup>-1</sup>	$WS$	Wind speed, m s <sup>-1</sup>
$F_{DLM}$	Deep lake mixing, m <sup>3</sup> month <sup>-1</sup>	$\delta_E$	Isotopic composition of evaporation, ‰
$F_R$	Rainfall on catchment, m <sup>3</sup> month <sup>-1</sup>	$\alpha^*$	Reciprocal of $\alpha$ , ‰ <sup>-1</sup>
$F_{SM}$	Catchment snowmelt, m <sup>3</sup> month <sup>-1</sup>	$\delta_L$	Isotopic composition of the lake surface, ‰
$F_{SSI}$	Surface soil infiltration, m <sup>3</sup> month <sup>-1</sup>	$h_n$	Normalized relative humidity, %
$F_{SSE}$	Surface soil evapotranspiration, m <sup>3</sup> month <sup>-1</sup>	$\delta_A$	Isotopic composition of atm. moisture, ‰
$F_{SSD}$	Surface soil drainage to deep soil, m <sup>3</sup> month <sup>-1</sup>	$\epsilon_{tot}$	Total isotopic separation, ‰
$F_{DSE}$	Deep soil evapotranspiration, m <sup>3</sup> month <sup>-1</sup>	$\epsilon_{eq}$	Equilibrium isotopic separation, ‰
$F_{RO}$	Catchment runoff, m <sup>3</sup> month <sup>-1</sup>	$\epsilon_k$	Kinetic isotopic separation, ‰
$F_{DSD}$	Deep soil drainage, m <sup>3</sup> month <sup>-1</sup>	$\epsilon_{s-a}$	Saturation vapor pressure–air, millibars
$F_{SF}$	Snowfall, m <sup>3</sup> month <sup>-1</sup>	$\epsilon_{s-w}$	Saturation vapor pressure–water, millibars
$T_a, T_w$	Air temperature, water temperature, °C	$\alpha$	Equilibrium isotopic fractionation factor, ‰
$CA$	Catchment area, m <sup>2</sup>	$C$	Kinetic isotopic separation value, ‰

(Eq. 11), and, ultimately, losses to subsurface flow (Eq. 15) and/or runoff (Eq. 16) to the lake. Within the model, this mass balance is defined by two reservoir and flux systems:

$$\frac{dRES_{SS}}{dt} = F_{SSI} - F_{SSE} - F_{SSD} \quad (5)$$

$$\frac{dRES_{DS}}{dt} = F_{SSD} - F_{DSE} - F_{DSD} \quad (6)$$

where  $RES_{SS}$  and  $RES_{DS}$  are the volumes of water stored within surface and deeper soil reservoirs, and  $F_{SSI}$ ,  $F_{SSE}$ ,  $F_{SSD}$ , and  $F_{DSE}$  (Eqs. 11–14) denote surface soil infiltration from precipitation, evapotranspiration from the soil surface, surface soil drainage to the deep soil reservoir, and evapotranspirative loss from deep soil, respectively. Any water in excess of the aforementioned fluxes is assumed to recharge a so-called inflow reservoir ( $RES_{IN}$ , Eq. 7, below) via deep soil drainage ( $F_{DSD}$  in Eq. 6, above, and Eq. 7).  $RES_{IN}$  is not meant to represent a reservoir in nature but rather is an empirical construct designed to allow the model to simulate water transport along slower flow paths.

Hydrologic mass balance within the inflow reservoir is also controlled by runoff ( $F_{RO}$ ) generated by catchment rainfall ( $F_R$ , Eq. 9) and/or melt of the catchment snowpack ( $F_{SM}$ , Eqs. 9, 10) in excess of soil water storage:

$$\frac{dRES_{IN}}{dt} = F_{RO} + F_{DSD} - F_{IN} \quad (7)$$

with the entire balance of excess water ultimately reaching the lake via combined surface and subsurface inflows ( $F_{IN}$ ) following a fixed retention time (i.e., residence time) in the catchment (identified as an inflow delay constant,  $C_{IN}$ , described below). Catchment snow cover (i.e., snowpack

reservoir size,  $RES_{SP}$ ) is determined simply by a balance between accumulation and melt:

$$\frac{dRES_{SP}}{dt} = F_{SF} - F_{SM} \quad (8)$$

where  $F_{SF}$  is snowfall and  $F_{SM}$  is a temperature-controlled snowmelt flux component based on the model of Vassiljev et al. (1995):

$$F_{SF} = \begin{cases} F_R & T_a \leq 0 \\ 0 & T_a > 0 \end{cases} \quad (9)$$

$$F_{SM} = \begin{cases} 0.021(-2 - T_a) \times CA \times dt^{-1} & RES_{SP} > 0.021(-2 - T_a) \times CA \\ RES_{SP} & RES_{SP} \leq 0.021(-2 - T_a) \times CA \\ RES_{SP} \times dt^{-1} & \end{cases} \quad (10)$$

wherein snowfall is generated at air temperatures ( $T_a$ ) less than or equal to 0°C, and melt occurs at temperatures greater than -2°C at a rate equivalent to 21 mm per °C per month.

*Infiltration, runoff, and inflow model subroutines*—The two-layer soil model subroutine (introduced above, in Eqs. 5, 6) controls the partitioning of catchment water between soil storage, runoff, and subsurface flow. This system of equations is derived, in part, from the two-layer soil models of Palmer (1965) and Vassiljev et al. (1995). Within the subroutine, surface soil infiltration ( $F_{SSI}$ ) occurs with rainfall ( $F_R$ ) and/or snowmelt ( $F_{SM}$ ) until the maximum available water capacity of the catchment is reached (i.e., the surface soil and deep soil reservoirs are saturated) according to the following equations:

$$F_{\text{SSI}} = \begin{cases} F_R + F_{\text{SM}} & RES_{\text{SS}} < CA \times AWC_{\text{SS}} \\ (F_R + F_{\text{SM}}) 0.5 & RES_{\text{SS}} \geq CA \times AWC_{\text{SS}} \\ & \text{and } RES_{\text{DS}} < CA \times AWC_{\text{DS}} \\ 0 & RES_{\text{SS}} \geq CA \times AWC_{\text{SS}} \\ & \text{and } RES_{\text{DS}} \geq CA \times AWC_{\text{DS}} \end{cases} \quad (11)$$

where  $CA$  is the area of the catchment and  $AWC_{\text{SS}}$  and  $AWC_{\text{DS}}$  are the surface soil and deep soil layer available water capacities. With saturation of the surface soil and undersaturation of the deep soil, catchment water is partitioned evenly (i.e.,  $F_{\text{SSI}} = (F_R + F_{\text{SM}}) 0.5$ , above) between surface soils and runoff (Eq. 16). When available water capacity is maximized in both reservoirs, soil water infiltration ceases ( $F_{\text{SSI}} = 0$ ).

Evapotranspirative flux from the soil surface ( $F_{\text{SSE}}$ ) is determined by potential evapotranspiration ( $PET$ , Eq. 23) and the total availability of water stored within the catchment:

$$F_{\text{SSE}} = \begin{cases} CA \times PET \times dt^{-1} & RES_{\text{SS}} > CA \times PET \\ RES_{\text{SS}} \times dt^{-1} & RES_{\text{SS}} \leq CA \times PET \end{cases} \quad (12)$$

When the surface soil water reservoir exceeds total catchment  $PET$ , evapotranspiration from surface soils occurs at the potential rate and excess water infiltrates deep soil. In contrast, evapotranspiration is reduced from the potential value to the volume of the surface soil water reservoir if  $PET$  demand is not met.

Water in excess of surface soil evapotranspiration ( $F_{\text{SSE}}$ ) and available water capacity ( $AWC_{\text{SS}}$ ) is transferred into the underlying deep soil layer from the overlying surface soil layer ( $RES_{\text{SS}}$ ) according to the equation:

$$F_{\text{SSD}} = (RES_{\text{SS}} - CA \times AWC_{\text{SS}}) \times dt^{-1} \quad (13)$$

where, again,  $F_{\text{SSD}}$  is the surface soil drainage flux. The deep soil layer reservoir, in turn, is subject to evapotranspirative losses in step with evapotranspiration from the surface soil reservoir:

$$F_{\text{DSE}} = \begin{cases} (CA \times PET \times dt^{-1}) - F_{\text{SSE}} & RES_{\text{DS}} > \\ & CA \times PET - F_{\text{SSE}} \times dt \\ RES_{\text{DS}} \times dt^{-1} & RES_{\text{DS}} \leq \\ & CA \times PET - F_{\text{SSE}} \times dt \end{cases} \quad (14)$$

Any water remaining within the deep soil layer in excess of evapotranspiration demand and available water capacity ( $AWC_{\text{DS}}$ ) is then transferred to the inflow reservoir (Eq. 7) as a deep soil drainage flux ( $F_{\text{DSD}}$ ):

$$F_{\text{DSD}} = (RES_{\text{DS}} - CA \times AWC_{\text{DS}}) \times dt^{-1} \quad (15)$$

All catchment precipitation and snowmelt is directly transferred to the lake inflow reservoir,  $RES_{\text{IN}}$ , as runoff,  $F_{\text{RO}}$ , under conditions of both surface and deep soil saturation ( $RES_{\text{SS}} \geq CA \times AWC_{\text{DS}}$  and  $RES_{\text{DS}} \geq CA \times$

$AWC_{\text{DS}}$ ). Under conditions of surface soil saturation and deep soil layer undersaturation, catchment precipitation and snowmelt is evenly partitioned as a flux to the inflow reservoir as runoff (i.e.,  $F_{\text{RO}} = (F_R + F_{\text{SM}}) 0.5$ ) and a flux of water to the deep soil layer ( $F_{\text{SSD}}$ , Eq. 13, above). No runoff is generated when surface soil layer water stores fall below available water capacity:

$$F_{\text{RO}} = \begin{cases} F_R + F_{\text{SM}} & RES_{\text{SS}} \geq CA \times AWC_{\text{SS}} \\ & \text{and } RES_{\text{DS}} \geq CA \times AWC_{\text{DS}} \\ (F_R + F_{\text{SM}}) 0.5 & RES_{\text{SS}} \geq CA \times AWC_{\text{SS}} \\ & \text{and } RES_{\text{DS}} < CA \times AWC_{\text{DS}} \\ 0 & RES_{\text{SS}} < CA \times AWC_{\text{SS}} \end{cases} \quad (16)$$

The flux of surface water runoff and deep soil water ( $F_{\text{IN}}$ ) from the inflow reservoir ( $RES_{\text{IN}}$ ) to the lake, then, is governed by the equation:

$$F_{\text{IN}} = RES_{\text{IN}} \times C_{\text{IN}} \times dt^{-1} \quad (17)$$

where the inflow delay constant,  $C_{\text{IN}}$ , is empirically derived through the model calibration process described below (see Catchment model calibration).

*Lake mixing model and outseepage subroutines*—To approximate the effects of seasonal stratification on surface water isotope content, a two-layer (surface and deep) lake model was developed in which the volume of each layer is controlled by monthly mixing depths determined from observations of lake temperature and salinity profiles over a 3-yr period.

The seasonal cycle of lake surface water evolution starts in midfall when evaporation rates decrease, rain saturates the surface soil, and the first runoff of the hydrologic year occurs. In the late fall, the onset of lake freezing leads to the formation of a low-salinity ice layer that thickens throughout the winter and early spring, until thaw and ice breakup occur. At this time, runoff and subsurface inflow from rainfall and snowmelt contribute isotopically light, low-salinity water to the lake surface layer while wind action begins to force mixing with the isotopically heavy deep lake water layer below. By midspring, the influx of freshwater begins to decrease and increasing evaporation rates result in renewed isotopic enrichment of the lake surface layer.

To simulate this process, the thickness of the lake surface water layer is independently controlled by a time dependent mixing component that is applied to the hypsographic relationships. This mixing component defines surface layer volume at any total lake depth and at any time of year, with the resulting difference between surface layer volume and total volume defining the volume of the deep layer. In this way, the total volume of the lake is always equal to the sum of the deep layer and surface layer volumes. In the late fall, the surface layer thickness is “reset” to zero for 3 months, which forces all water into the deep lake reservoir. This has the effect of completely mixing the lake and, due to the small influx of water from the catchment during this time, leads to surface water isotope values approximately equal to that of

runoff. The equations that govern the flow between the surface and deep layers are described as follows:

$$F_{\text{SLM}} = \begin{cases} 0 & M < 9 \\ RES_{\text{SL}} \times dt^{-1} & M \geq 9 \end{cases} \quad (18)$$

$$F_{\text{DLM}} = \begin{cases} (SVC - RES_{\text{SL}}) \times dt^{-1} & M < 9 \\ 0 & M \geq 9 \end{cases} \quad (19)$$

where  $M$  is the month (0–11, with 0 = January and 11 = December) and  $SVC$  is surface lake volume control determined by lake stratification profiles.

Outseepage from the lakes is determined strictly as a function of lake volume and outseepage rate estimates:

$$F_{\text{SOS}} = C_{\text{SR}} \times RES_{\text{SL}} \times dt^{-1} \quad (20)$$

$$F_{\text{DOS}} = C_{\text{SR}} \times RES_{\text{DL}} \times dt^{-1} \quad (21)$$

*Lake evaporation and catchment evapotranspiration model subroutines*—The evaporation and evapotranspiration models applied in this study are the simplified versions of the modified Penman equations proposed by Valiantzas (2006) and are described as follows:

$$E = \left[ 0.051(1 - ALB) \times R_s \times (T_a + 9.5)^{(1/2)} - 2.4 \left( \frac{R_s}{R_a} \right)^2 + 0.052(T_a + 20) \times \left( 1 - \frac{RH}{100} \right) \times (a_u - 0.38 + 0.54WS) \right] \times 30 \quad (22)$$

$$PET = \left[ 0.051(1 - ALB) \times R_s \times (T_a + 9.5)^{(1/2)} - 2.4 \left( \frac{R_s}{R_a} \right)^2 + 0.048(T_a + 20) \times \left( 1 - \frac{RH}{100} \right) \times (0.5 + 0.536WS) \right] \times 30 \quad (23)$$

where  $E$  and  $PET$  are evaporation and potential evapotranspiration in  $\text{mm day}^{-1}$ ,  $ALB$  is the albedo of the lake (0.08, Eq. 22) and surrounding grass (0.25, Eq. 23) surfaces,  $T_a$  is average daily temperature in  $^{\circ}\text{C}$ ,  $R_s$  is average daily incoming solar radiation in  $\text{MJ m}^{-2} \text{d}^{-1}$ ,  $R_a$  is average daily extraterrestrial radiation in  $\text{MJ m}^{-2} \text{d}^{-1}$ ,  $RH$  is average daily relative humidity expressed as a percentage,  $a_u$  is the Penman wind function constant, and  $WS$  is average daily wind speed in  $\text{m s}^{-1}$  ( $E$  and  $PET$  values are set to zero when  $T_a \leq 0$ ). This simplified version of the Penman equation was chosen on the basis of available meteorological data and the fact that, when applied to small lakes in seasonal climatic settings, it produces results that compare favorably to those of the energy budget method for calculating evaporation (Rosenberry et al. 2007a,b). Note that  $E$  and  $PET$  values are multiplied by 30 in order to convert from daily to monthly estimates.

*Isotope mass-balance equations*—The reservoir and flux structure of the isotope mass-balance model is identical to that of the hydrologic model and follows the equations of Dincer (1968), Gonfiantini (1986), and Gat (1995). Within the model, oxygen and hydrogen isotope values, in standard delta ( $\delta$ ) notation as the per mil (‰) deviation from Vienna standard mean ocean water, are calculated for each reservoir at each time step and are multiplied by the corresponding hydrologic flux to determine the isotope mass balance of any given water mass.

The isotopic composition of moisture evaporating from the lake surface ( $\delta_E$ ) is estimated by the linear resistance model of Craig and Gordon (1965):

$$\delta_E = \frac{\alpha^* \delta_L - h_n \delta_A - \varepsilon_{\text{tot}}}{1 - h_n + 0.001 \varepsilon_{\text{kin}}} \quad (24)$$

where  $\alpha^*$  is the reciprocal of the equilibrium isotopic fractionation factor,  $\delta_L$  is the isotopic composition of lake water,  $h_n$  is the ambient humidity normalized to lake water temperature,  $\delta_A$  is the isotopic composition of atmospheric moisture,  $\varepsilon_{\text{tot}}$  is the total per mil isotopic separation ( $\varepsilon_{\text{eq}} + \varepsilon_k$ ),  $\varepsilon_{\text{eq}}$  is the equilibrium isotopic separation, and  $\varepsilon_k$  is the kinetic isotopic separation.

Normalized relative humidity is calculated from the saturation vapor pressure of the overlying air ( $e_{s-a}$ ) and the saturation vapor pressure at the surface water temperature ( $e_{s-w}$ ) in millibars:

$$h_n = RH \times \frac{e_{s-a}}{e_{s-w}} \quad (25)$$

$$e_{s-a} \text{ and/or } e_{s-w} = 6.108 \exp \left( \frac{17.27T}{T + 237.7} \right) \quad (26)$$

Atmospheric moisture ( $\delta_A$ ) is assumed to be at isotopic equilibrium with precipitation (Gibson et al. 2002):

$$\delta_A = \delta_P - \varepsilon_{\text{eq}} \quad (27)$$

The equilibrium isotopic fractionation factor ( $\alpha$ ) and the reciprocal of the equilibrium isotopic fractionation factor ( $\alpha^*$ ) for oxygen (28) and hydrogen (29) are calculated using the equations of (Horita and Wesolowski 1994):

$$\ln \alpha = 0.35041 \times \left( \frac{10^6}{T_w^3} \right) - 1.6664 \times \left( \frac{10^3}{T_w^2} \right) + 6.7123 \left( \frac{1}{T_w} \right) - 7.685 \times 10^{-3} \quad (28)$$

$$\ln \alpha = 1.1588 \times \left( \frac{T_w^3}{10^9} \right) - 1.6201 \times \left( \frac{T_w^2}{10^6} \right) + 0.79484 \times \left( \frac{T_w}{10^3} \right) + 2.9992 \times \left( \frac{10^6}{T_w^3} \right) - 161.04 \times 10^{-3} \quad (29)$$

$$\alpha^* = 1/\alpha \quad \alpha^* < 1 \quad (30)$$

where  $T_w$  is the temperature (degrees K) of the lake surface water. The per mil equilibrium isotopic separation ( $\varepsilon_{\text{eq}}$ ) of

oxygen and hydrogen follows accordingly:

$$\varepsilon_{\text{eq}} = 1000 \times (1 - \alpha^*) \quad (31)$$

Kinetic fractionation ( $\varepsilon_k$ ) is controlled by molecular diffusion and the moisture deficit ( $1 - h_n$ ) over the lake surface (Merlivat and Jouzel 1979):

$$\varepsilon_k = C \times (1 - h_n) \quad (32)$$

where  $C$  is the experimentally derived isotopic separation value of 14.3‰ for oxygen and 12.4‰ for hydrogen (Vogt 1976; Araguás-Araguás et al. 2000) and  $h_n$  is the humidity normalized to the temperature of the lake surface water.

*Model inputs*—Steady state and continuous model simulations used monthly and daily weather data from two sites located within  $\sim 10$  km and 200 m elevation of CL and SL. Specifically, average monthly temperature and precipitation were calculated using  $\sim 100$  yr of data from National Climatic Data Center weather stations at Omak (1930 to present) and Conconully (1900 to present). Monthly and daily average values for relative humidity and wind speed, and daily average values for solar insolation were derived from 20 yr of data collected at Omak by the Pacific Northwest Cooperative Agricultural Weather (AgriMet) Network. All climate input data were linearly corrected using 2 yr of daily Campbell Scientific weather station data from CL. Monthly average values for incoming solar radiation were calculated using the method of Valiantzas (2006). One year (2007) of lake water temperature measurements from Solinst Leveloggers were used to derive monthly surface water temperature offsets from average air temperature. Monthly  $\delta^{18}\text{O}$  and  $\delta D$  values of precipitation were estimated using the interpolated values of Bowen and Wilkinson (2002), Bowen and Revenaugh (2003), and Bowen et al. (2005) and were adjusted in the temperature sensitivity tests by 0.6‰ per  $1^\circ\text{C}$  according to Rozanski et al. (1992).

Catchment surface areas were estimated from georeferenced topographic maps (U.S. Geological Survey 1981) using geographic information system (GIS) software. Specific soil types and their corresponding areas within each catchment were identified from U.S. Department of Agriculture regional soil report maps and then used to calculate a weighted average available water capacity ( $AWC$ ) for each catchment.

Lake volume–surface area and lake volume–depth relationships were derived from detailed bathymetric surveys completed in 2007. Depth and location data were collected with a combination global positioning system receiver and chartplotter (Garmin GPSMAP 430S). All data were compiled, gridded, and contoured using three-dimensional surface mapping software (Surfer, Golden Software). Best-fit polynomial regression curves were then applied to the software generated hypsographic profiles to produce equations of depth and surface area as a function of lake volume.

*Lake and climate monitoring data*—Water samples for oxygen and hydrogen isotope analyses were collected from the shorelines of SL and CL, from shallow wells within the

lake catchments, and from nearby streams at irregular intervals between June 2005 and November 2008. Isotopic ratios of lake water were measured at the University of Arizona Environmental Isotope Laboratory by  $\text{CO}_2$  equilibration with a VG602C Finnigan Delta S isotope ratio mass spectrometer. The reported precision is 0.1‰ for  $\delta^{18}\text{O}$  and 1.0‰ for  $\delta D$ . Lake level at both SL and CL was measured with a Solinst Levelogger data logger and corrected for barometric pressure changes recorded by a land-based Solinst Barologger device. Each Levelogger was tied to floats and positioned at the center of each lake approximately 1 m below the surface using anchored ropes. Barologger devices were positioned in the shade approximately 10 m above the lake surfaces. A Campbell Scientific weather station was deployed near the shoreline approximately 3 m above the lake surface of CL in May of 2006. Air temperature, relative humidity, barometric pressure, wind speed and direction, precipitation, and solar insolation were measured at 30 s intervals and recorded every 30 min.

## Results

All model simulations were conducted with the Stella software using the fourth order Runge-Kutta numerical integration method. In the first series of model simulations (*see Seepage estimation simulations*), monthly average climate data and modern catchment parameter datasets were used to approximate the monthly and seasonal variability of CL and SL water levels, lake water  $\delta^{18}\text{O}$  values, and outseepage rates. In the second sequence of model simulations (*see Catchment model calibration*), outseepage estimates derived from the first set of simulations were combined with continuous daily meteorological data and initial catchment reservoir volumes and characteristics (Table 1) to simulate lake level and  $\delta^{18}\text{O}$  values over the 3-yr lake water sampling and monitoring period (2005–2008). Results from these simulations were compared to observations in order to calibrate the catchment submodel. The model was then adapted to simulate lake water  $\delta D$  evolution over the same 3-yr period in order to independently test the validity of the isotopic submodel. The third series of simulations (*see Model sensitivity to climate variables*) used both the outseepage estimates derived from the first set of model tests and the model calibration factor developed from the second set of tests to evaluate the sensitivity of the lakes to each of the primary drought controlling climate variables (i.e., precipitation, relative humidity, and temperature).

*Seepage estimation simulations*—Initially, outseepage was assigned a value of zero and both lakes were assumed to lose water only by evaporation. In this configuration, evaporative losses were insufficient to balance lake levels and surface water  $\delta^{18}\text{O}$  values at or near modern values. Outseepage rates were subsequently increased in a stepwise manner until average annual lake level matched modern observations for both CL and SL (Figs. 3, 4).

Simulations of modern lake level were achieved only by removing  $1.5\% \pm 0.3\%$  and  $0.5\% \pm 0.3\%$  of monthly lake volume through outseepage at CL and SL, respectively. At

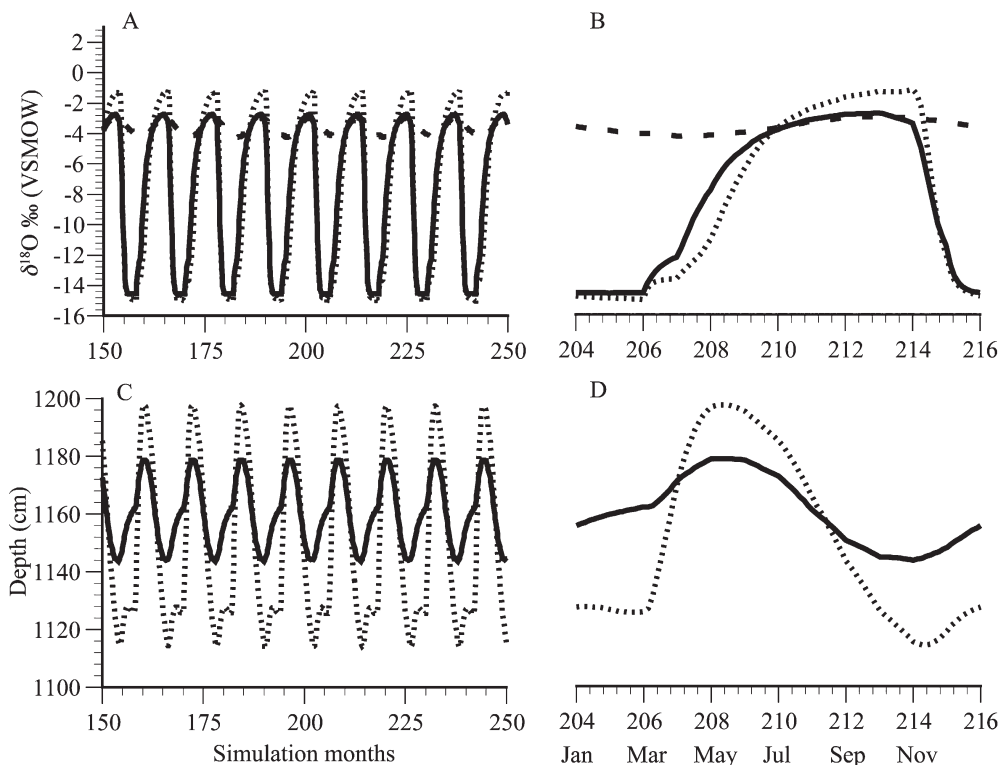


Fig. 3. (A) Simulated Castor Lake steady state total water column  $\delta^{18}\text{O}$  values (coarse dashed line) and surface water  $\delta^{18}\text{O}$  values (solid line) with delayed catchment water inflow. Fine dashed line depicts surface water  $\delta^{18}\text{O}$  values without delayed inflow. (B) Expanded view of Castor Lake  $\delta^{18}\text{O}$  values between model months 204 (January) and 215 (December) from Fig. 3A. (C, D) Simulated Castor Lake steady state lake-level change with (solid lines) and without (fine dashed lines) delayed inflow.

these outseepage rates, after applying catchment calibration factors (see *Catchment model calibration*), the simulated lake-level curves reproduced the observed pattern of seasonal water level change ( $\sim 0.4$  m) at both sites, with lowest lake levels occurring between October and November and highest lake levels occurring between May and July. The model also reproduced the observed seasonal variations in lake surface water  $\delta^{18}\text{O}$  ( $\sim 12\text{‰}$  for CL and  $\sim 17\text{‰}$  for SL), with minimum values between November and January and maximum values between July and October. Outseepage estimates were insensitive to catchment calibration, with almost identical average annual lake levels resulting from both calibrated and uncalibrated model configurations.

*Catchment model calibration*—The objectives of the second set of simulations were to define the inflow delay constant ( $C_{\text{IN}}$ ), in order to calibrate the catchment model, and to refine outseepage estimates. These simulations used 3 yr (August 2005 to October 2008) of daily climate data from the CL and Omak AgriMet weather stations and initial values for model reservoirs based on steady state values and depth and surface water  $\delta^{18}\text{O}$  measurements taken in late July of 2005. In these experiments, an inflow delay constant (Eq. 17) was applied to each catchment in an effort to simulate expected delays between rainfall and snowmelt within the catchment and lake inflow. The applied inflow delay constant was sequentially adjusted downward from a value of one (i.e., no delay in the transport of water from the

catchment to the lake) until the differences between the predicted seasonal lake level and  $\delta^{18}\text{O}$  values and the observed lake level and  $\delta^{18}\text{O}$  values were minimized (Fig. 5). After defining the inflow delay constant (0.21), outseepage estimates were adjusted within the range defined by the seepage estimation simulations in order to improve model calibration. Final outseepage estimates were 1.6% and 0.7% of monthly volume for CL and SL, respectively. At both CL and SL, the inflow delay constant that resulted in lake-level values most closely matched that observations equates to a catchment residence time of  $\sim 140$  d.

The model was also adapted to predict lake water hydrogen isotope variability over the 3-yr sampling and monitoring period used for model calibration (Fig. 5). Modeled lake surface water  $\delta D$  values were similar to measured  $\delta D$  values and produced a theoretical local evaporation line (LEL) with a slope similar to that derived from lake surface water measurements (Fig. 2). The ability of the model to simulate hydrogen isotope variability within both CL and SL demonstrates that the improvements in accuracy resulting from calibration are not specific to the oxygen isotope system and that the structure of the hydrologic and isotopic model is widely applicable.

*Model sensitivity to climate variables*—The objective of the third series of simulations was to determine the hydrologic and isotopic sensitivity of SL and CL to temperature, relative humidity, and precipitation changes.

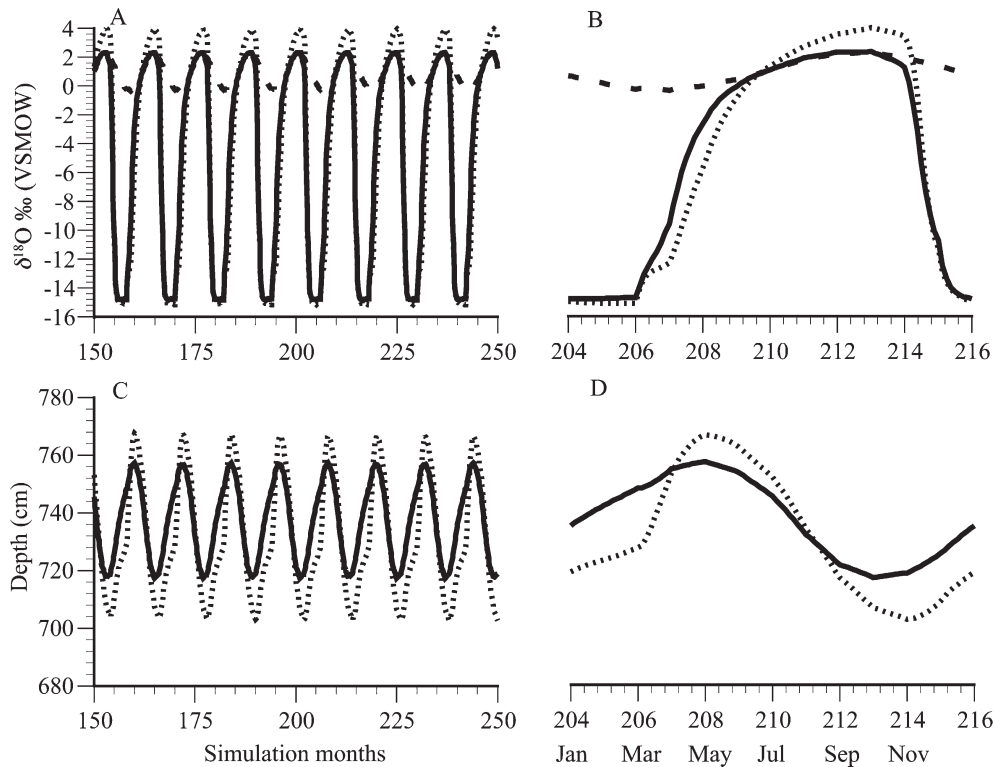


Fig. 4. Simulated Scanlon Lake steady state total water column  $\delta^{18}\text{O}$  values (coarse dashed line) and surface water  $\delta^{18}\text{O}$  values (solid line) with delayed catchment water inflow. Fine dashed line depicts surface water  $\delta^{18}\text{O}$  values without delayed inflow. (B) Expanded view of Scanlon Lake  $\delta^{18}\text{O}$  values between model months 204 (January) and 215 (December) from Fig. 4A. (C, D) Simulated Scanlon Lake steady state lake-level change with (solid lines) and without (fine dashed lines) delayed inflow.

In each set of sensitivity tests, simulations were conducted on a monthly time step over  $\sim 110$  model years using modern catchment parameters and average climate data for the 20th century. Between the 501st and 1004th simulation month, corresponding to the beginning (October) of the 42nd and end (September) of the 84th model hydrologic year, respectively, the tested climate parameter was either increased or decreased in a stepwise manner by a constant percentage determined on the basis of the coefficient of variation of the parameter over the 20th century (Table 2).

**Temperature sensitivity tests**—Atmospheric temperature can influence lake hydrologic and isotopic balance by altering evaporative flux from the lake surface, catchment evapotranspiration rates, water column temperature and stratification, normalized *RH* values, and through direct control of the liquid–vapor equilibrium fractionation factor for evaporating water (Eqs. 22–32). At mid- and high-latitude sites, atmospheric temperature also influences the isotopic composition of lake water through its effect on the isotopic composition of precipitation (Rozanski et al. 1992).

Atmospheric temperatures 20% above or below average 20th century values resulted in water depth changes of less than  $\pm 0.35$  m at SL and less than  $\pm 0.20$  m at CL (Table 4), suggesting that basin hydrology at both sites is relatively insensitive to temperature changes. Oxygen isotope value shifts of  $\sim 1.2\text{‰}$  at both SL and CL, resulting from a 20% temperature change, were largely a

consequence of temperature control on the isotopic composition of precipitation and to a lesser extent on changes in hydrologic and isotopic fluxes.

**Relative humidity sensitivity tests**—The sensitivity of lakes to changes in relative humidity is largely due to the effect of *RH* on the kinetic fractionation process that occurs during evaporation from the lake surface. Relative humidity also influences lake hydrologic balance by affecting evapotranspiration rates. The hydrologic response of both lakes to a 10% change in *RH* was relatively small (less than  $\sim 0.3$  m) in comparison to the change in lake water  $\delta^{18}\text{O}$  values ( $\pm 1.1\text{‰}$  and  $\pm 0.5\text{‰}$  at SL and CL, respectively; Table 4), indicating that *RH* sensitivity is primarily a result of isotope fractionation processes rather than hydrologic influence on lake water isotopic composition. Additionally, the more pronounced isotopic response of SL to *RH* changes (relative to CL, a nearly 0.6‰ difference) suggests that lake sensitivity is in part controlled by the proportion of water lost through evaporation, with greater evaporative loss at SL resulting in greater sensitivity to *RH* forcing (see evaporative outflow proportion discussion and figures below).

**Precipitation sensitivity tests**—Precipitation rates were incrementally adjusted from 50% to 150% of modern values, reflective of the coefficient of variation of recorded precipitation over the 20th century. In response to a 50%

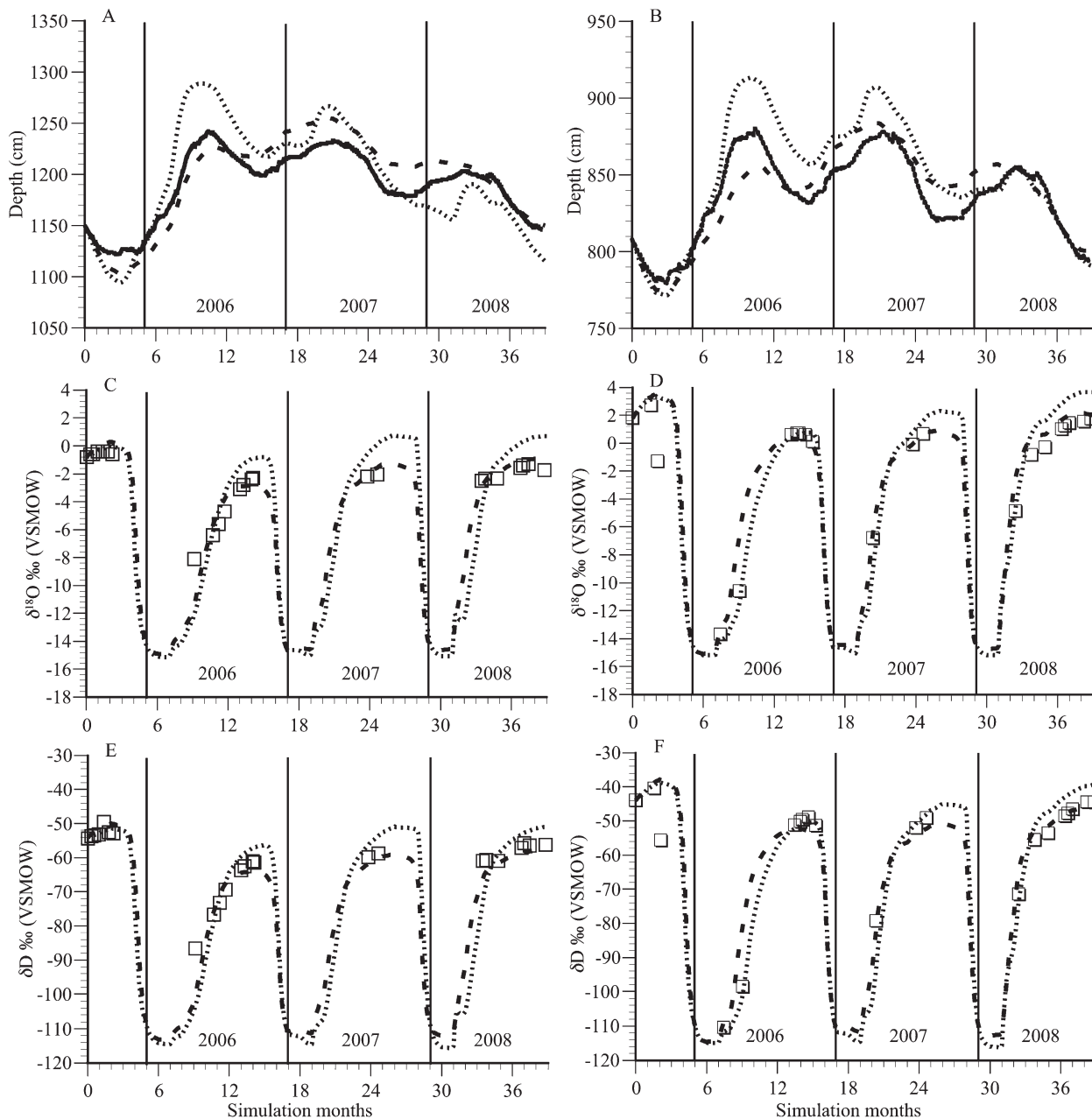


Fig. 5. (A, B) Castor Lake and Scanlon Lake calibrated (coarse dashed lines) and uncalibrated (fine dashed lines) lake-level simulations using continuous input data plotted with observed lake-level changes (solid lines). (C, D) Castor Lake and Scanlon Lake calibrated (coarse dashed lines), uncalibrated (fine dashed lines), and measured (open squares) lake surface water  $\delta^{18}\text{O}$  values between August 2005 and October 2008. (E, F) Castor Lake and Scanlon Lake calibrated (coarse dashed lines), uncalibrated (fine dashed lines), and measured (open squares) lake surface water  $\delta D$  values.

Table 4. Relative humidity and temperature sensitivity test results (Summer [June, July, August] averages).

	Model year	Castor Lake				Scanlon Lake			
		Temperature -20%	Temperature +20%	RH -10%	RH +10%	Temperature -20%	Temperature +20%	RH -10%	RH +10%
$\delta^{18}\text{O}$ (‰)	40	-3.6	-3.6	-3.6	-3.6	1.4	1.4	1.4	1.4
	82	-4.8	-2.5	-3.2	-4.1	0.2	2.5	2.3	0.3
Depth (cm)	40	1162	1162	1162	1162	739	739	739	739
	82	1179	1145	1135	1189	771	715	714	770

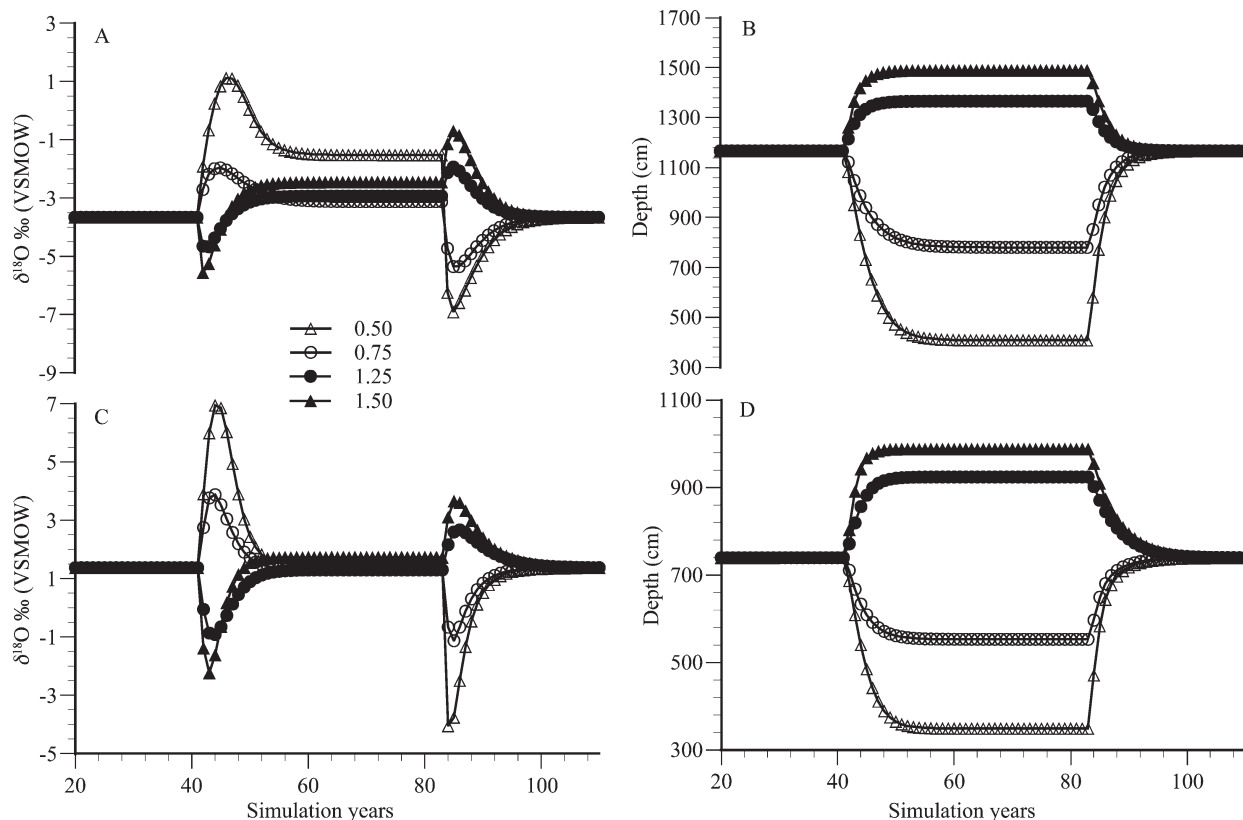


Fig. 6. (A) Castor Lake average summer month (June, July, August) surface water  $\delta^{18}\text{O}$  values and (B) lake levels from precipitation sensitivity tests. (C) Scanlon Lake average summer month (June, July, August) surface water  $\delta^{18}\text{O}$  values and (D) lake levels from precipitation sensitivity tests.

reduction in precipitation, both SL and CL exhibited a marked, but transient (i.e., short-lived)  $\delta^{18}\text{O}$  increase of  $\sim 5.6\text{‰}$  and  $\sim 4.8\text{‰}$ , respectively, with CL taking longer to achieve initial maxima and steady state  $\delta^{18}\text{O}$  values relative to SL, due in part to the larger volume and consequently slower response time of CL (Fig. 6). Increased precipitation levels (50% above modern) resulted in transient  $\delta^{18}\text{O}$  decreases of  $\sim 1.9\text{‰}$  and  $\sim 3.6\text{‰}$  at CL and SL, respectively.

## Discussion

*The influence of hypsography and seepage on lake water  $\delta^{18}\text{O}$  values*—In the increased precipitation simulations, both CL and SL achieved initial, transient  $\delta^{18}\text{O}$  minima and steady state values relatively quickly (in comparison with the precipitation reduction scenarios) largely as a result of a rapid increase in lake surface area with increasing depth. Moreover, the transient isotopic response was stronger in the decreased precipitation scenarios because of the longer hydrologic equilibration times resulting from relatively gradual decreases in lake surface area with decreasing depth (Fig. 6).

Under all precipitation scenarios SL exhibited a steady state  $\delta^{18}\text{O}$  value that was similar to the value prior to hydrologic forcing (differences ranged from about  $-0.1$  to  $0.4\text{‰}$ ). In contrast, CL exhibited a steady state value that was considerably different (by as much as  $2.1\text{‰}$ ) than the value prior to forcing, and, in the case of the  $+25\%$  and

$+50\%$  precipitation scenarios, opposite in sign of the transient response (i.e., an increase in steady state water  $\delta^{18}\text{O}$  values occurred as a result of a lake-level increase). This apparently contradictory response results from control of lake steady state isotopic response to hydrologic forcing by surface area to volume (SA:V) ratio variation with changing depth and the consequent change in the proportions of water lost through fractionating (evaporation) and nonfractionating (outseepage) hydrologic pathways. For example, in lakes such as SL with a high SA:V ratio (i.e., shallow lakes with a proportionally large surface area), the outseepage rate ( $C_{\text{SR}}$  in the model) is less influential in determining the proportion of water lost through evaporation because at all depths the SA:V ratio is high. As a consequence, evaporation is the only significant outflow pathway and steady state lake water  $\delta^{18}\text{O}$  values are buffered only slightly by outflow through seepage. To that end, as volumetric adjustments occur at SL in response to hydrologic forcing, minimal changes occur in the proportion of water lost through evaporation (relative to outseepage), thereby resulting in effectively negligible changes in steady state isotopic values (Fig. 7). At CL, however, the lower overall SA:V ratio and the higher outseepage rate cause the opposite response, in that lake volumetric changes resulting from hydrologic forcing lead to larger proportional changes in water loss through evaporation vs. outseepage and consequently substantial variations in steady state  $\delta^{18}\text{O}$  values (Fig. 8). Roberts et al.

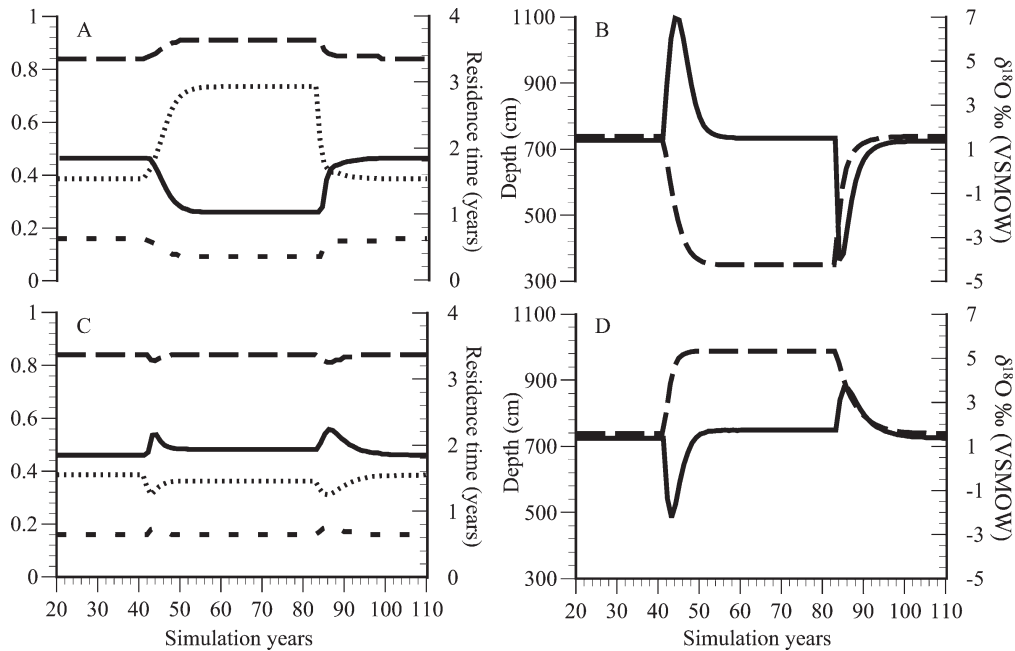


Fig. 7. Scanlon Lake water residence time (solid line), SA : V ratio (fine dashed line), and percentage of outflow via seepage (medium dashed line) and evaporation (coarse dashed line) changes resulting from (A) a 50% decrease and (C) a 50% increase in precipitation. Scanlon Lake surface water  $\delta^{18}O$  values (solid line) and lake-level changes (coarse dashed line) resulting from (B) a 50% decrease and (D) a 50% increase in precipitation.

(2008) predicted similar results (i.e., lakes with appreciable outseepage respond more strongly at steady state to hydrologic forcing) using a schematic model for differential lake response to common water balance forcing.

The influence of the SA : V ratio on steady state lake water  $\delta^{18}O$  values was examined at SL through steady state sensitivity simulations in which outseepage rates were increased to 2.4% of monthly volume (Fig. 9A,B) and, at

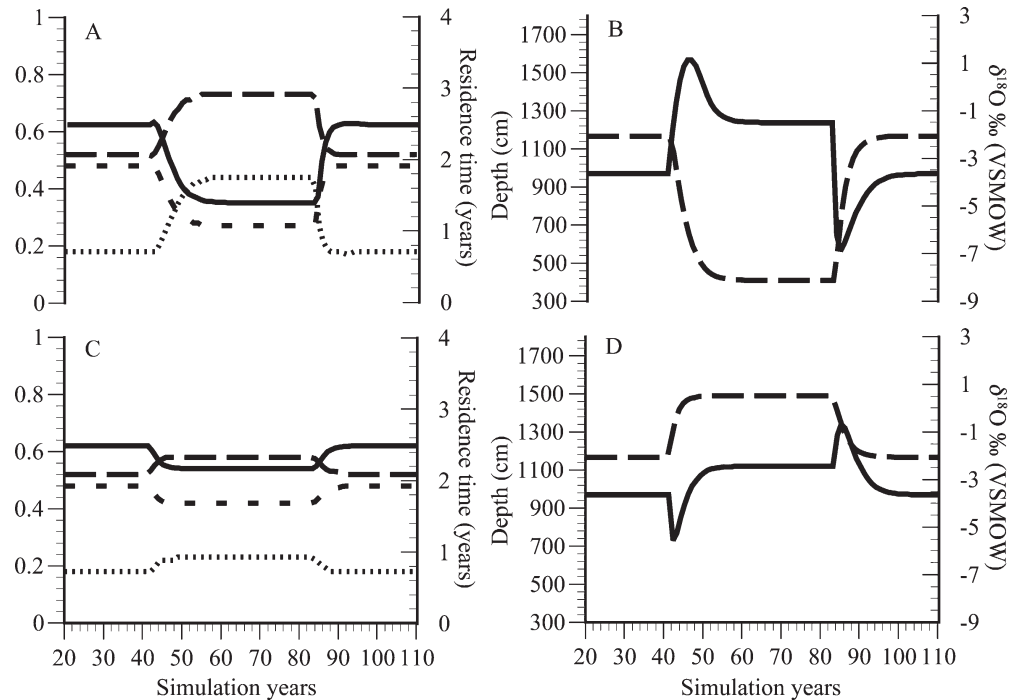


Fig. 8. Castor Lake water residence time (solid line), SA : V ratio (fine dashed line), and percentage of outflow via seepage (medium dashed line) and evaporation (coarse dashed line) changes resulting from (A) a 50% decrease and (C) a 50% increase in precipitation. Castor Lake surface water  $\delta^{18}O$  values (solid line) and lake-level changes (coarse dashed line) resulting from (B) a 50% decrease and (D) a 50% increase in precipitation.

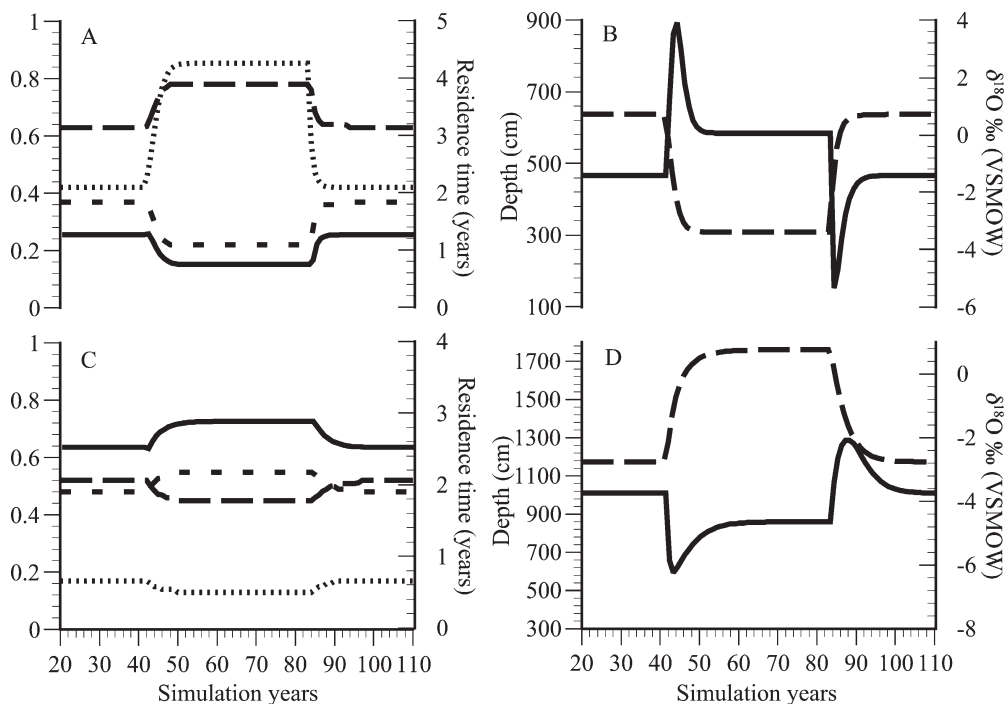


Fig. 9. (A) Scanlon Lake water residence time (solid line), SA:V ratio (fine dashed line), and percentage of outflow via seepage (medium dashed line) and evaporation (coarse dashed line) changes resulting from a 50% decrease in precipitation and outseepage increased from 0.7% to 2.4% of monthly lake volume, and (B) consequent lake water  $\delta^{18}\text{O}$  values (solid line) and lake-level changes (coarse dashed line). (C) Castor Lake water residence time (solid line), SA:V ratio (fine dashed line), and percentage of outflow via seepage (medium dashed line) and evaporation (coarse dashed line) changes resulting from a 50% increase in precipitation and hypsography altered such that the SA:V ratio decreases with depths above 12 m. (D) Consequent lake water  $\delta^{18}\text{O}$  values (solid line) and lake-level changes (coarse dashed line).

CL, through altered hypsographic profiles such that the SA:V ratio decreased with increasing depth above 12 m (Fig. 9C,D). In these configurations, precipitation was decreased by 50% at SL and increased by 50% at CL. At SL, the increased outseepage rate simulation resulted in a large increase in the steady state  $\delta^{18}\text{O}$  value ( $\sim 1.3\text{‰}$ ). The positive direction of the isotopic response was a result of the increase in the SA:V ratio over the depth interval of the test. At CL, the altered SA:V ratio led to a steady state isotopic response (nearly  $-0.9\text{‰}$ ) with a sign opposite (i.e., negative) that of the original configuration due to the decrease in the percentage of outflow via evaporation resulting from the altered SA:V ratio.

*Residence time response to hydrologic forcing*—Changes in the SA:V ratio also explain, in part, estimated changes in lake water residence time at CL and SL in response to hydrologic forcing. As lake volume increases, surface area increases to a proportionally greater extent, causing greater volumetric loss through evaporation, a larger outflow-to-volume ratio, and hence a lower residence time. At both SL and CL, for example, a 50% decrease in precipitation results in a substantial increase in the SA:V ratio, and a corresponding decrease in residence time (defined as total lake volume divided by total outflux) as the loss of water through evaporation from the lake surface increases relative to lake volume (Figs. 7A, 8A). At both sites, there is an inverse relationship between the

SA:V ratio and residence time, regardless of the volumetric response to hydrologic forcing.

*Seepage model considerations*—In all model simulations, water loss via seepage was determined strictly as a percentage of total lake volume (Eqs. 20, 21). At both SL and CL, estimated outseepage fell within the range of values calculated using Darcy's law and generally accepted lake sediment hydraulic conductivity values between  $10^{-8}$  and  $10^{-9}$   $\text{m s}^{-1}$ . However, given that lake sediment hydrologic parameters can vary between the littoral and benthic zones and that seepage rates often decrease exponentially with distance offshore, this simple model for calculating outseepage may not be appropriate in some lakes and may lead to lake level and lake water  $\delta^{18}\text{O}$  predictions that differ from observation (Genereux and Bandopadhyay 2001). For example, in lakes with highly permeable littoral zone sediments, an increase in lake level resulting from a hydrologic forcing could result in a decrease in steady state  $\delta^{18}\text{O}$  values regardless of the SA:V ratio change (Almendinger 1990). In lake systems with heterogeneous sediments, outseepage responses to hydrologic forcing may therefore exert greater control on steady state  $\delta^{18}\text{O}$  values than lake hypsography.

Numeric mass-balance models can accurately predict the hydrologic and isotopic evolution of small, closed-basin lake systems on seasonal and interannual timescales when calibrated using modern lake water stratification, surface water isotopic composition, and lake-level change data. At

Scanlon and Castor Lakes, north-central Washington, mass-balance model sensitivity tests demonstrate a strong lake water hydrologic and transient isotopic response to precipitation changes. Neither relative humidity nor temperature strongly influence lake hydrologic responses, but they do affect steady state lake water  $\delta^{18}\text{O}$  values via controls on kinetic and equilibrium isotope fractionation.

The results presented here describe how the isotopic composition of closed-basin lake water is dependent on both initial conditions and input forcing and show that specific lake water  $\delta^{18}\text{O}$  values cannot always be ascribed to specific lake hydrologic states. A related inference is that, within an individual lake, the magnitude of the transient isotopic response is at least partly controlled by how quickly the equilibrium lake level and corresponding surface area can be reached, with longer equilibration times resulting in stronger transient isotopic responses. Most importantly, these results demonstrate the potential for inconsistent isotopic responses to drought and/or pluvial conditions between adjacent closed-basin lakes with differing outseepage rates and lake basin morphologies.

Semiquantitative interpretations of lake sediment  $\delta^{18}\text{O}$  records often rely on a somewhat overly simplistic model in which steady state increases (decreases) in closed-basin lake volume resulting from climatically induced changes in precipitation–evaporation balance cause steady state decreases (increases) in closed-basin lake water  $\delta^{18}\text{O}$  values. This model is based on several assumptions, most notably that lake basin geometry is approximately conic and, as a consequence, the SA:V ratio decreases with increasing depth (Benson et al. 1996). This study demonstrates that closed-basin lake steady state isotopic responses are dependent upon interactions between both lake outseepage and basin morphology and that in lakes with nonstandard geometry (i.e., in which the SA:V ratio increases with increasing depth) this basic model relating hydrologic forcing and isotopic response may not apply.

This study also suggests that closed-basin lakes with minimal outseepage will likely exhibit a transient isotopic response to stochastic variability in hydrologic forcing but will not strongly respond to variations in mean hydrologic conditions (i.e., mean precipitation, relative humidity and temperature control of catchment hydrologic inputs to the lake). Conversely, closed-basin lakes with appreciable outseepage and a SA:V ratio that changes with depth will exhibit a strong isotopic response to both stochastic variability in hydrologic forcing and variations in mean hydrologic conditions, with the direction of the SA:V ratio change (either positive or negative with increasing depth) controlling the direction of the steady state isotopic response. These relationships provide a mechanism for explaining inconsistencies in multiproxy sediment records from regional closed-basin lakes and highlight the need for caution when applying only semiquantitative models to explain the relationship between climatic forcing and oxygen isotope values in sediments from underdetermined lake systems.

#### Acknowledgments

We thank Nathan Stansell, Chris Helander, Jeremy Moberg, Broxton Bird, and John Riedal for assistance in the field. Stacey

Levine and Dan Nelson provided valuable comments on earlier drafts of the manuscript. We also thank three anonymous reviewers for thoughtful remarks on the text. This work was funded by the National Science Foundation Earth System History program grant ATM-0401948 and small grants from the Geological Society of America and the University of Pittsburgh's Henry Leighton Memorial Scholarship and International Studies Fund.

#### References

- ALMENDINGER, J. E. 1990. Groundwater control of closed-basin lake levels under steady-state conditions. *J. Hydrol.* **112**: 293–318, doi:10.1016/0022-1694(90)90020-X
- ARAGUÁS-ARAGUÁS, L., K. FROELICH, AND K. ROZANSKI. 2000. Deuterium and oxygen-18 isotope composition of precipitation and atmospheric moisture. *Hydrol. Process.* **14**: 1341–1355, doi:10.1002/1099-1085(20000615)14:8<1341::AID-HYP983>3.0.CO;2-Z
- BENSON, L., AND F. PAILLET. 2002. HIBAL: A hydrologic-isotopic-balance model for application to paleolake systems. *Quat. Sci. Rev.* **21**: 1521–1539, doi:10.1016/S0277-3791(01)00094-4
- , L. D. WHITE, AND R. RYE. 1996. Carbonate deposition, Pyramid Lake Subbasin, Nevada: 4. Comparison of the stable isotope values of carbonate deposits (tufas) and the Lahontan lake-level record. *Palaeogeogr. Palaeoclimatol. Palaeoecol.* **122**: 45–76, doi:10.1016/0031-0182(95)00099-2
- BOWEN, G. J., AND J. REVENAUGH. 2003. Interpolating the isotopic composition of modern meteoric precipitation. *Water Resour. Res.* **39**: 1299, doi:10.1029/2003WR002086., doi:10.1029/2003WR002086
- , L. I. WASSENAAR, AND K. A. HOBSON. 2005. Global application of stable hydrogen and oxygen isotopes to wildlife forensics. *Oecologia* **143**: 337–348, doi:10.1007/s00442-004-1813-y, doi:10.1007/s00442-004-1813-y
- , AND B. WILKINSON. 2002. Spatial distribution of  $\delta^{18}\text{O}$  in meteoric precipitation. *Geology* **30**: 315–318, doi:10.1130/0091-7613(2002)030<0315:SDOIM>2.0.CO;2
- BRYSON, R. A., AND K. F. HARE. 1974. Climates of North America, p. 5–12. *In* H. E. Landsberg [ed.], *World survey of climatology*. Elsevier Scientific.
- CRAIG, H., AND L. I. GORDON. 1965. Isotopic oceanography: Deuterium and oxygen 18 variations in the ocean and the marine atmosphere. *Mar. Geochem. Occas. Publ.* **3**: 277–374.
- DINCER, T. 1968. The use of oxygen 18 and deuterium concentrations in the water balance of lakes. *Water Resour. Res.* **4**: 1289–1306.
- GAT, J. R. 1995. Stable isotopes in fresh and saline lakes, p. 139–165. *In* A. Lerman, D. M. Imboden and J. R. Gat [eds.], *Physics and chemistry of lakes*. Springer-Verlag.
- GENEREUX, D., AND I. BANDOPADHYAY. 2001. Numerical investigation of lake bed seepage patterns: Effects of porous medium and lake properties. *J. Hydrol.* **241**: 286–303, doi:10.1016/S0022-1694(00)00380-2
- GIBSON, J. J., E. E. PREPAS, AND P. MCEACHERN. 2002. Quantitative comparison of lake throughflow, residency, and catchment runoff using stable isotopes: Modeling and results from a regional survey of Boreal lakes. *J. Hydrol.* **262**: 128–144, doi:10.1016/S0022-1694(02)00022-7
- GONFIANTINI, R. 1986. Environmental isotopes in lake studies, p. 113–168. *In* P. Fritz and J. C. Fontes [eds.], *Handbook of environmental geochemistry*, vol. 2: The terrestrial environment. B. Elsevier Science.
- HORITA, J., AND D. WESOLOWSKI. 1994. Liquid-vapour fractionation of oxygen and hydrogen isotopes of water from the freezing to the critical temperature. *Geochim. Cosmochim. Acta* **47**: 3425–3437, doi:10.1016/0016-7037(94)90096-5

- HOSTETLER, S. W., AND P. J. BARTLEIN. 1990. Simulation of lake evaporation with application to modeling lake variations of Harney-Malheur Lake, Oregon. *Water Resour. Res.* **26**: 2603–2612.
- , AND L. V. BENSON. 1994. Stable isotopes of oxygen and hydrogen in the Truckee River-Pyramid Lake surface-water system. 2. A predictive model of  $\delta^{18}\text{O}$  and  $\delta^2\text{H}$  in Pyramid Lake. *Limnol. Oceanogr.* **39**: 356–364.
- JONES, M. D., C. N. ROBERTS, AND M. J. LENG. 2007. Quantifying climatic change through the last glacial-interglacial transition based on lake isotope palaeohydrology from central Turkey. *Quat. Res.* **67**: 463–473, doi:10.1016/j.yqres.2007.01.004
- MERLIVAT, L., AND J. JOUZEL. 1979. Global climatic interpretation of the deuterium-oxygen 18 relationship for precipitation. *J. Geophys. Res.* **84**: 5029–5033, doi:10.1029/JC084iC08p05029
- PALMER, W. C. 1965. Meteorological drought. Weather Bureau Research Paper 45. U.S. Department of Commerce.
- ROBERTS, N., AND OTHERS. 2008. Stable isotope records of Late Quaternary climate and hydrology from Mediterranean lakes: The ISOMED synthesis. *Quat. Sci. Rev.* **27**: 2426–2441, doi:10.1016/j.quascirev.2008.09.005
- ROSENBERRY, D. O., T. C. WINTER, D. C. BUSO, AND G. E. LIKENS. 2007a. Comparison of 15 evaporation methods applied to a small mountain lake in the northeastern USA. *J. Hydrol.* **340**: 149–166, doi:10.1016/j.jhydrol.2007.03.018
- , ———, ———, AND ———. 2007b. Reply to comment by J. Szilagyi on “Comparison of 15 evaporation methods applied to a small mountain lake in the northeastern USA” [*J. of Hydrol.* 340 (3–4) (2007) 149–166]. *J. Hydrol.* **348**: 566–567, doi:10.1016/j.jhydrol.2007.09.050
- ROSENMEIER, M. F., M. BRENNER, D. A. HODELL, J. B. MARTIN, AND M. W. BINFORD. In Press. Quantitative assessments of Holocene environmental change in Petén, Guatemala: Predictive models of catchment hydrology and lake water  $\delta^{18}\text{O}$  values. *Quat. Res.*
- ROWE, H. D., AND R. B. DUNBAR. 2004. Hydrologic-energy balance constraints on the Holocene lake-level history of lake Titicaca, South America. *Clim. Dynam.* **23**: 439–454, doi:10.1007/s00382-004-0451-8.
- ROZANSKI, K., L. ARAGUÁS-ARAGUÁS, AND R. GONFIANTINI. 1992. Relation between long-term trends of oxygen-18 isotope composition of precipitation and climate. *Science* **258**: 981–985, doi:10.1126/science.258.5084.981
- SACKS, L. A. 2002. Estimating ground-water inflow to lakes in central Florida using the isotope mass-balance approach. U.S. Geological Survey Water Resources Investigations Report 02-4192.
- SHAPLEY, M. D., E. ITO, AND J. J. DONOVAN. 2008. Isotopic evolution and climate paleorecords: Modeling boundary effects in groundwater-dominated lakes. *J. Paleolimnol.* **39**: 17–33, doi:10.1007/s10933-007-9092-3
- U.S. GEOLOGICAL SURVEY. 1981. “Riverside, Washington” map. 1:24,000. 7.5 minute series [Internet]. Reston (VA): U.S. Geological Survey [accessed 2010 January 13]. Available from <http://rocky.ess.washington.edu/data/raster/drg/okanogan/index.html>.
- VALIANTZAS, J. D. 2006. Simplified versions for the Penman evaporation equation using routine weather data. *J. Hydrol.* **331**: 690–702, doi:10.1016/j.jhydrol.2006.06.012
- VASSILJEV, J., S. P. HARRISON, AND A. HAXELTINE. 1995. Recent lake-level and outflow variations at Lake Viljandi, Estonia: Validation of a coupled lake-catchment modeling scheme for climate change studies. *J. Hydrol.* **170**: 63–77, doi:10.1016/0022-1694(95)02691-H
- VOGT, H. J. 1976. Separation of isotopes in the evaporation of water. Staatsexamensarbeit, Universität Heidelberg.

Associate editor: Roland Psenner

Received: 10 July 2009

Accepted: 21 November 2009

Amended: 05 January 2010